GEOLOGICA CARPATHICA, 2025, 76, 1, 23–36 https://doi.org/10.31577/GeolCarp.2025.02

Geochronological constraints on the Karakoram Metamorphic Complex, Hunza Valley, Pakistan: Zircon and monazite dating of Tethyan collision events

RAFIQUE AHMAD[1,2,3,✉], ASGHAR ALI[1], ONDREJ NEMEC[2], MARIÁN PUTIŠ[2] and PATRIK KONEČNÝ[4]

[1]Department of Geology, University of Peshawar, Peshawar-25130, Pakistan
[2]Department of Mineralogy, Petrology and Economic Geology, Faculty of Natural Sciences, Comenius University, Bratislava, Ilkovičova 6, 842 15 Bratislava, Slovakia
[3]Department of Geology, Bacha Khan University Charsadda, Charsadda-24420, Pakistan
[4]State Geological Institute of Dionýz Štúr, Mlynská dolina 1, 817 04 Bratislava, Slovakia

(Manuscript received February 13, 2025; accepted in revised form April 23, 2025; Associate Editor: Igor Broska)

Abstract: U–Pb zircon and U–Th–Pb EPMA monazite dating of one metamafic sample and two metapelitic samples are studied from Karakoram Metamorphic Complex, Hunza NW Pakistan. These new geochronological results address the collision–related metamorphic evolution of the thickened Asian Plate crust with the Kohistan Island Arc and then with the Indian Plate. Following the collision and accretion of the Kohistan Island Arc during the Late Cretaceous, the Karakoram Metamorphic Complex experienced crustal thickening and sillimanite–grade metamorphism at the southern apex. Two new chronological events have been recorded in the investigated Hunza Valley region. U–Pb zircon ages of 103.1±2.9 Ma and 100.0±5.3 Ma represent the peri–plutonic thermal metamorphism before the India–Asia collision, whereas U–Th–Pb monazite age of 47±4.3 Ma documents the peak sillimanite grade metamorphism with ongoing India–Asia collision. These zircon ages of the metamorphic crystallization are inferred to be related to the subduction of the Tethys Ocean beneath the southern Asian margin which finally led to the south-ward collisional thrusting of the Cretaceous Hunza Plutonic Unit of the Karakoram Batholith in the Hunza Valley over the Karakoram Metamorphic Complex in the Eocene. Crustal thickening and the metamorphic evolution from sillimanite to kyanite to staurolite grade and granitoid magmatism are related with the Kohistan Island Arc–Asia and the India–Asia collision zones.

Keywords: Main Karakoram Thrust, Karakoram Metamorphic Complex, Hunza Valley, zircon and monazite dating

Introduction

Karakoram–Hindu Kush–Lhasa and Qiangtang orogenic terranes formed due to episodic collision between the Kohistan Island Arc and amalgamated southernmost margin of the Asian plate followed by the final collision of the Indian Plate and complete closure of the Tethyan Ocean (Searle et al. 1999; Palin et al. 2012; Larson et al. 2019; Soret et al. 2019). The Karakoram terrane of the Gondwana affinity is nicely exposed in Pakistan that provides a natural laboratory to understand syn and post tectonic magmatism, multiple phases of metamorphism and deformations associated with sequential collision of plates and closing of the intervening oceans (Gaetani 1997; Hildebrand et al. 1998, 2000, 2001). The dextral Karakoram Fault separates the Karakoram terrane from the southern Tibet (Mahar et al. 2014). The Rushan–Pshart Suture Zone separates the Karakoram from the Hindu Kush, whereas the Shyok Suture Zone, also termed the Main Karakoram Thrust (MKT), delineates the southern plate boundary with the Kohistan Island Arc (Searle 2011).

✉ corresponding author: Rafique Ahmad
rafique.ahmad@bkuc.edu.pk

Three successive subduction related tectonic events have been documented in the Karakoram terrane. The Karakoram basement rocks are intruded by the Cretaceous calc–alkaline axial batholith (Crawford & Searle 1992; Debon & Khan 1996). This event led to the Shyok back-arc basin formation in the Mid-Cretaceous (Rolland et al. 2000, 2002). The complete closure of the intervening Paleo-Tethys between the Late Cretaceous Kohistan Island Arc and Karakoram terrane is characterized by the formation of the Shyok Suture Zone (Petterson & Windley 1992; Weinberg et al. 2000). The final closure of the Neo-Tethys in the Eocene caused crustal thickening, mid crustal anatectic melting and amphibolite facies metamorphism in the Karakoram terrane. Crustal thickening, metamorphic episodes from sillimanite to kyanite to staurolite grade metamorphism and magmatism are related with the Kohistan Island Arc–Asia and India–Asia collision zones (Searle et al. 1989, 2010; Lemennicier et al. 1996; De Sigoyer et al. 2000; Fraser et al. 2001; Rolland et al. 2001; Green et al. 2008).

The Karakoram Metamorphic Complex (KMC) preserves a complex history of metamorphism and magmatism (Palin et al. 2012; Faisal et al. 2014; Mahar et al. 2014; Soret et al. 2019). However after Palin et al. (2012), further investigation is required to explain briefly the geochronological studies on amphibolite grade metamorphic rock units for tectonic evolution of the KMC. Pressure–temperature (P–T) conditions of metamorphic rocks can be calculated using phase equilibria modelling and metamorphic history preserved in zoned metamorphic index minerals (Palin et al. 2014; Soret et al. 2019). Metamorphic history of multiply deformed rocks can be plotted on P–T pseudosection using zircon and garnet geochemistry (Foster et al. 2000, 2002; Kohn et al. 2005; Larson et al. 2011). In pelitic rocks heavy rare earth elements (HREEs) dominantly partitioned into garnet as compare to monazites (Pyle et al. 2001; Corrie & Kohn 2008). During synchronous growth of garnet and monazite HREEs partitioning into garnet have important tectonic implications to interpret the monazite petrochronology and garnet growth (Kohn et al. 2005; Corrie & Kohn 2008; Larson et al. 2019). The partitioning of HREEs and light rare earth elements (LREEs) between garnet and monazite gives constrain on syn- versus post-metamorphic growth of garnets in the pelitic rocks. Past thermochronological investigation of the KMC has utilized U–Pb dating techniques from garnet porphyroblasts containing staurolite inclusions with accessory minerals include apatite, ilmenite, rutile, zircon and tourmaline (Searle et al. 2010). During this previous study, the P–T conditions of 648±30 °C and 7.7 ±1.8 kbar and 22±0.3 Ma for monazite growth age were interpreted as the timing of peak metamorphism from kyanite-grade pelite in the Panmah–Braldu confluence region. Similarly, the samples from garnet amphibolite orthogneiss in Bullah dome (northeast of Hunza valley) yielded 766±54 °C and 11.9±1.5 and 28.0±1.7 Ma and Dassu orthogneiss in Dassu gneiss dome (east of Hunza valley) produced 689±48 °C and 5.7±1.9 kbar and 5.4±0.1 Ma (Fraser et al. 2001; Searle et al. 2010).

Why we used monazite dating from metamorphic rocks? Monazite is a common accessory mineral in peraluminous metapelitic rocks (Spear & Pyle 2002) which is widely used for geochronology as it has the tendency for having higher concentrations of U and Th (Kohn & Malloy 2004). Similarly monazite is also characterized by low initial absorptions of common Pb (Parrish 1990). Monazite also shows enormous resilience to U–Th–Pb internal diffusion at temperature less than 900 °C (Cherniak et al. 2004). This is governed by multiple stages of growth recorded within multiply deformed metamorphosed rocks (e.g., Kohn et al. 2005). Appearance and growth of metamorphic monazite in pelitic rocks during prograde metamorphism at the staurolite or kyanite isograd is aided by the coeval breakdown of allanite and P-bearing phases such as apatite (Wing et al. 2003; Kohn & Malloy 2004; Yang & Pattison 2006; Janots et al. 2008). Such monazite growth condition is mostly possible in lower/middle amphibolite facies rocks. Further, the presence of monazite as inclusions in garnet may help in understanding the age interpretation for porphyroblast growth during amphibolite facies metamorphism. This scenario assumes that monazite recrystallization has not taken place due to later fluid penetration along micro-fractures in the host mineral (e.g., Carson et al. 2004). According to some studies, the high grade metamorphic conditions responsible for partial melting to occur, the pre-existing monazite becomes unstable and easily dissolve into early formed silicate melt, recrystallizing on melt solidification (e.g., Hawkins & Bowring 1999; Rubatto et al. 2001; Kohn et al. 2005). Though the laboratory experiments results show that monazite has a somewhat low solubility in peraluminous rocks (e.g., Rapp & Watson 1986) and so prograde monazite has the ability to be preserved together with younger grains that are associated to partial melting progressions.

In this contribution, we present a new U–Pb zircon and U–Th–Pb EPMA monazite geochronological investigation of specimens collected along the Hunza Valley in the Karakoram region. Monazite and zircon ages revealed two (Cretaceous and Eocene) collision events recorded in KMC in the Karakoram terrane of northwest Pakistan (Fig. 1). These new age data help close a gap in our understanding of the tectonic evolution of the southernmost plate margin of the Karakoram terrane in the Karakoram Block. For this purpose we used 3 representative samples for our study. Samples RA–M–08 (Grt–Cpx–Hbd orthogeniss), RA–M–10 (metapelitic schist) and RA–M–41 (metapelitic schist) lie in the KMC (Fig. 1). The obtained results may serve for correlation studies of the Alpine–Carpathian and Himalayan Tethyan systems evolution.

Geological settings

The Karakoram Range, ~700 km long and 100×150 km wide, extends in a broad arc along the northern border of Afghanistan, Pakistan, India and the southern border of China (Fig. 1). Geological investigations in the Karakoram terrain show that the seismic activity in the upper mantle crust is low with occasional earthquakes at depth of 70–100 km (Chen & Molnar 1983) indicating that the upper mantle is cold (Brandon & Romanowicz 1986). Caporali (2000) showed that the axis of range agrees to a large negative gravity anomalies (<500 mGal) and extreme heat flow, which suggest the existence of strong basement similar to that present under Tibet today. Massive rock formation, uplift and erosion have created the highest Asian Plate and many deep crustal outcrops, several of which are equivalent exposures in the Tibet today. The rocks exposed between the Karakoram Batholith and Shyok Suture Zone or MKT to the south is considered the Karakoram Range (Searle & Tirrul 1991; Crawford & Searle 1993; Fraser et al. 2001; Rolland et al. 2001, 2006; Searle et al. 2010). The area in the KMC provides excellent exposure and has been the object of detailed studies in the past.

The lithology of KMC consists of marble, metamorphic marls and chalcosilicates with secondary metamudstone and orthogneiss (Searle et al. 1989; Searle 1991; Rolland et al. 2006). A brief summary of the geological evolution of the Karakoram Range is presented below; however, the subsequent discussion of metamorphic evolution is limited to metamorphic units due to their superior ability to modify the P–T–t

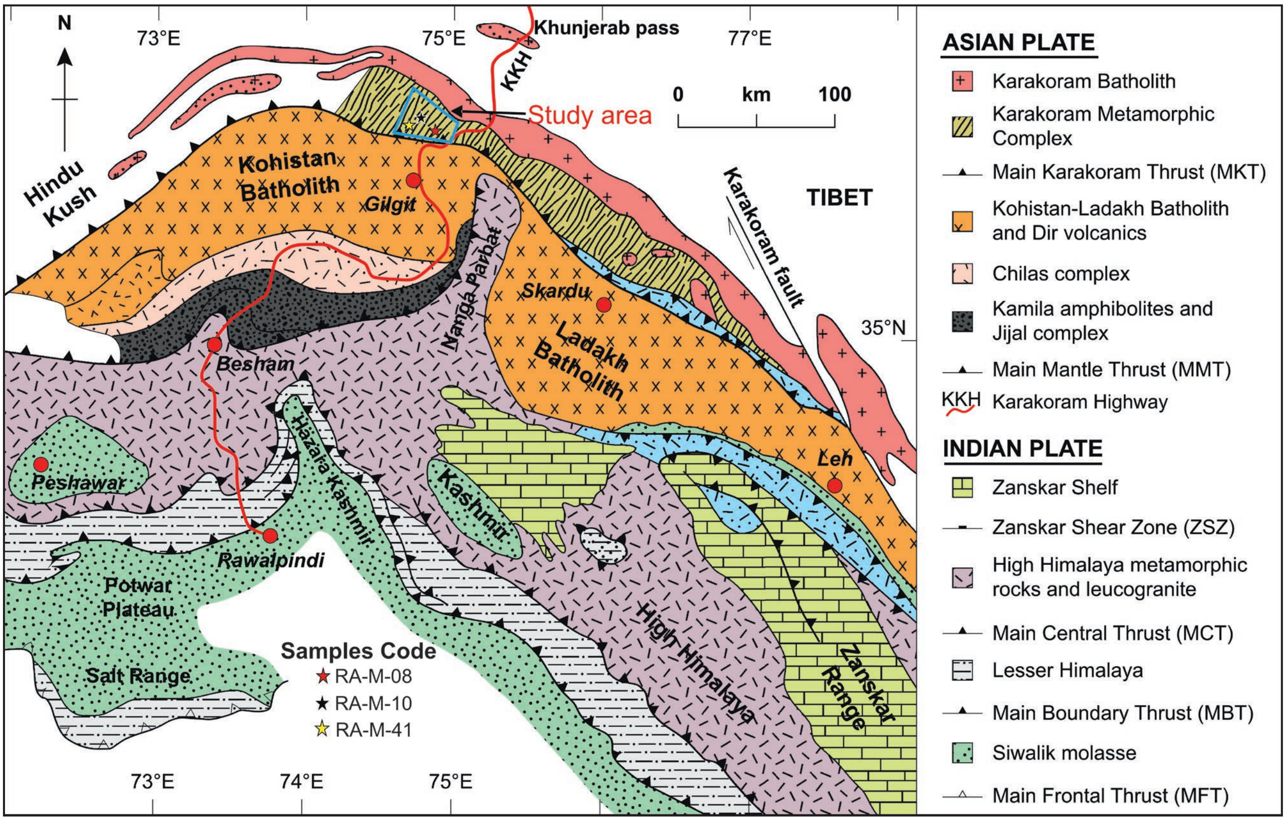

Fig. 1. Geological map of the north Pakistan showing different tectonic units (Searle et al. 1999). The samples are shown with different colored stars.

events. Subduction of the Tethys ocean towards the south Asian margin led to the formation of the Karakoram Batholith, a mixed intrusion of I–type granodiorite and monzogranite that crystallized between 120 and 180 Ma (Rb–Sr whole rock; Debon et al. 1987; Searle et al. 1992). Therefore, the rocks in Asia may have undergone high–temperature metamorphism (M0) associated with magma intrusion. Such magmatism ceased upon the closure of the Shyoke Suture and the accretion of the Kohistan Island Arc to the Asian margin (Mahéo et al. 2004). This accretion event resulting in a prolonged period of sillimanite grade metamorphism (M1) between c. 83 and c. 53 Ma (U–Pb monazite; Fraser et al. 2001; Foster et al. 2004). However, the lack of data severely limits the period of metamorphism before and after the Shyok Suture Zone closure; thus M0 and M1 may be a continuous event.

Following the consequent closure of the Indus Suture and beginning of the India–Asia collision, thrusting of rocks to the south-west caused in extensive crustal thickening and regional kyanite- and sillimanite-grade metamorphism (M2) between c. 50 and c. 22 Ma with peak metamorphic conditions ranging between 8–10 kbar and 600–700 °C (U–Pb monazite and zircon; Bertrand et al. 1988; Searle et al. 1989, 2010; Allen & Chamberlain 1991; Searle & Tirrul 1991; Lemennicier et al. 1996; Rolland et al. 2001). As a result, this event ended in the large scale crustal melting within the Baltoro region resulting in the formation of Baltoro Plutonic Unit (east of Hunza Valley) of Karakoram Batholith. The Baltoro Plutonic Unit composed of biotite monzogranite and garnet two-mica leucogranite with crystallization ages ranging between c. 25 and 13 Ma (U–Pb zircon and monazite; Parrish & Tirrul 1989; Schärer et al. 1990; Searle et al. 2010). Similarly in the meantime, the staurolite grade metamorphism (M3) occurred in the Hunza Valley at 16.0±1.0 Ma (U–Pb monazite; Fraser et al. 2001). The most recent episode of metamorphism and crustal melting (M4) is observed within the cores of the Bullah and Dassu gneiss domes in the Baltoro region, which contain sillimanite- and K-feldspar-grade migmatites (Rolland et al. 2001, 2006) that formed between 5.4±0.2 Ma (U–Pb monazite; Fraser et al. 2001) and 6.7±0.5 Ma (U–Pb monazite; Smith 1993) at pressures of 4–7.5 kbar (Villa et al. 1996). It can be seen from these data that significant differences exist in the magmatic–metamorphic evolution of the Hunza Valley and Baltoro regions.

Material and Methods

Zircon U–Pb dating

For the separation of zircon grains the samples were crushed and grinded using a jaw crusher and disk miller. The grinded samples were passed through 350 μm sieve to eliminate the coarser particles. In order to split the heavy minerals from <350 μm fragments the water shaking table was used. Frantz isodynamic magnetic separation technique was further adopted for heavy mineral fraction to efficiently clean it from magnetic materials. The remaining portions were passed through the heavy liquid (Di-iodomethane) to get the clean zircon fraction. Zircon grains were handpicked from both samples (RA–M–08 and RA–M–41) using a binocular microscope, mounted in epoxy resin, and polished to expose their surfaces.

To determine the age of metamorphism, U–Pb zircon dating of one metamafic (RA–M–08) and one metapellitic schist (RA–M–41) samples were carried out at the Geochronology and Tracers Facility (GTF) British Geological Survey (Nottingham, UK). For reference material sample BB9 $^{206}Pb/^{238}U$ age=573.2±4.2 (2σ, MSWD=1.17, n=18; Santos et al. 2017) and Temora 2 $^{206}Pb/^{238}U$ age=419.2±3.0 (2σ, MSWD=0.55, n=18; Black et al. 2004) were used in the current analyses.

All U–Pb analyses were performed on a Nu Attom single collector inductively coupled plasma mass spectrometer (SC–ICP–MS) coupled to a New Wave Research 193UC excimer laser ablation system fitted with a TV3 cell. Standard-sample bracketing was employed with the full setup and protocols described previously in Roberts et al. (2016) and full analytical data provided in the supporting information. All data and ages are shown and quoted at 2σ, are $^{206}Pb/^{238}U$ ages, and follow uncertainty propagation guidelines of Horstwood et al. (2016). The data are presented as common–Pb weighted mean plots and Tera–Wasserburg plots using a regression through the data anchored at a $^{207}Pb/^{206}Pb$ value of 0.84±0.02 based on Stacey & Kramers (1975).

Monazite analytical techniques (EPMA) and U–Th–Pb geochronology

To determine chemistry and metamorphic age of monazite, one metapelitic sample RA–M–10 was chosen with 45 analyzed spots in monazite grains to ensure the precision of the data. Geochronology of monazite was carried out by the monazite age reference correction (MARC) method developed by Konečný et al. (2018). This method is using microprobe analyses from the CAMECA SX 100 at the Dionýz Štúr State Geological Institute in Bratislava. The analyser was equipped with four wavelength-dispersive spectrometers (WDS). Before the analysis, thin section of more than 30 μm thickness was coated with a thin carbon film. Monazite spot analyses were acquired under 15 kV accelerating voltage, 180 nA beam current, and a 3 μm beam diameter with the aim of increasing both counting efficiency and spatial resolution. For MARC correction a set of 7 age monazite reference standards was measured for assessment of minor systematic errors that cannot be suppressed within currently used measuring procedure. These systematic errors are regardless of the number of accumulated analyses. Natural and synthetic standards were used for calibration of following elements and corresponding spectral lines: orthoclase (K Kα), wollastonite (Si Kα , Ca Kα), Al_2O_3 (Al Kα), hematite (Fe Kα), chromite (Cr Kα), SrTiO3 (Sr Lα), UO_2 (U Mβ), ThO_2 (Th Mβ), PbS (Pb Mα), $LaPO_4$ (La Lα), $CePO_4$ (Ce Lα), $PrPO_4$ (Pr Lβ), $NdPO_4$ (Nd Lβ), $SmPO_4$ (Sm Lβ), $EuPO_4$ (Eu Lβ), YPO_4 (Y Lα), $GdPO_4$ (Gd Lα), $TbPO_4$ (Tb Lα), $DyPO_4$ (Dy Lβ), $HoPO_4$ (Ho Lβ), $ErPO_4$ (Er Lβ), $TmPO_4$ (Tm Lα), $YbPO_4$ (Yb Lα), $LuPO_4$ (Lu Lβ), GaAs (As Lα), apatite (P Kα), barite (S Kα), Al_2O_3 (Al Kα) and wollastonite (Ca Kα). Long counting times were used to increase the analytical precision: for Pb (300 s peak and 2×150 s backgrounds), Th (35 s peak and 2×17.5 s background), U (80 s peak and 80 s background), and Y (40 s peak and 2×20 s background). Other details and principles of MARC dating technique can be found in Konečný et al. (2018).

Results

U–Th–Pb monazite-(Ce) chemistry and geochronology

Monazite crystals in sample RA–M–10 range from 20 to 50 μm in size. These grains are mostly found in association with foliation parallel phases such as biotite and plagioclase. The studied monazite grains are homogenous and lacking any internal zonation or overgrowth (Fig. 2). Monazite contains up to 4.4 to 8.7 mol.% of cheralite component $[Ca_2Th_2(PO_4)_4]$. Huttonite component $[Th(SiO_4)]$ is generally 1 mol.%, while the monazite content is ranging from 91.7 to 95 mol.% and is therefore dominated by monazite substitution (Fig. 3a, b; Table 1). The increase in Th concentration is compensated by elevated U and Y, i.e. 0.34–0.68 % UO_2, 1.62–2.39 % Y_2O_3.

Thorium and uranium concentration of monazite ranges from 1.86–4.37 and 0.31–0.59 wt.% respectively. Th/U ratios for monazite are showing low values of 4.39 to 12.52 typical of the metamorphic origin (Table 2). The Th+U+Si vs. P+Y+REE compositional plot for monazite spot analyses illustrates more restricted scatter towards monazite substitution vector (Fig. 3b).

In situ U–Th–Pb analyses of monazite grains was carried out for 14 grains from sample RA–M–10 (Fig. 4; Table 2). All the grains occurred in the main matrix of the sample with long axis generally parallel to the foliation, no monazite was observed in garnet. Chemical ages from 34 spot analyses of monazite grains range from 28 to 91 Ma yield a mean age of 47±4.3 Ma (Fig. 4a, b).

U–Pb zircon geochronology

Fifty four zircon grains (fourty six grains from sample RA–M–08 and eight grains from sample RA–M–41) were analyzed for U, Th and Pb isotopes using the LA–ICP–MS system. The zircon crystals contain relatively low amounts of uranium 12.5–291.7 ppm in RA–M–08 (Grt–Cpx–Hbd orthogeniss) and 10.0–74.6 ppm in RA–M–41 (metapelitic schist; Table 3), reliable with their lack of metamictization or

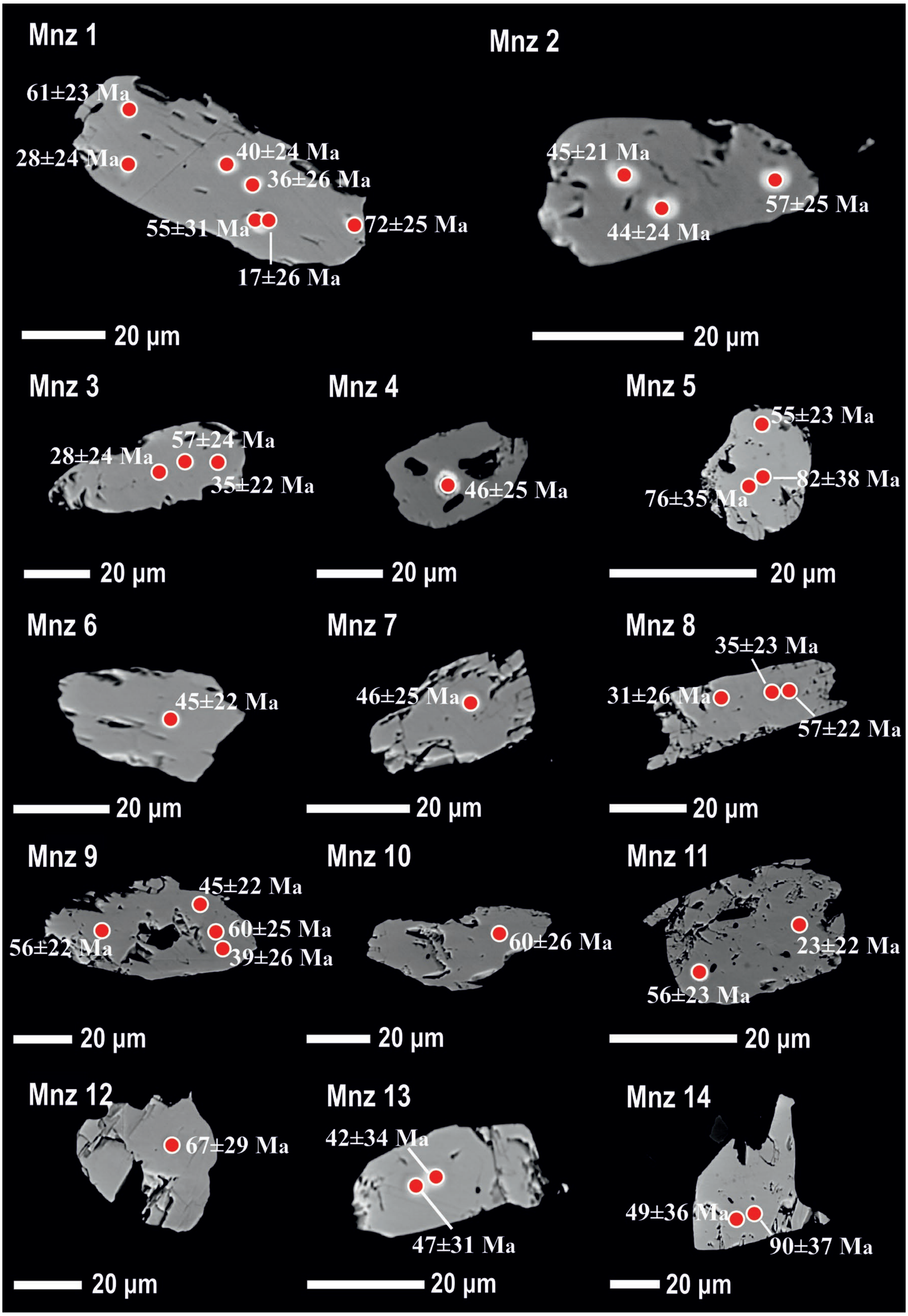

Fig. 2. Backscattered electrons (BSE) images of monazite grains from sample RA–M–10 with spot ages obtained by U–Th–Pb EPMA geochronology.

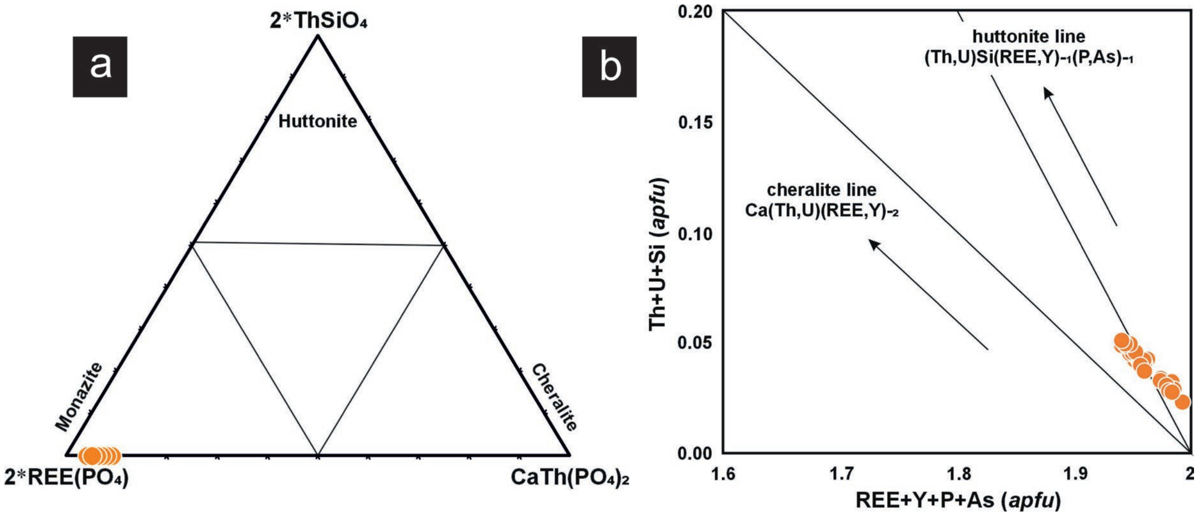

Fig. 3. a — Major substitutions: monazite–cheralite and monazite–huttonite. **b** — Compositions of monazite in terms of monazite, huttonite and cheralite molar fractions. Sample RA–M–10.

Table 1: EPMA chemical analyses of all monazite grains dated in sample RA–M–10.

Grain No.	**1**	**2**	**3**	**4**	**5**	**6**	**7**	**8**	**9**	**10**	**11**	**12**	**13**	**14**
An. No.	**1**	**2**	**1**	**1**	**3**	**1**	**1**	**1**	**3**	**1**	**1**	**1**	**2**	**2**
P_2O_5 (wt. %)	30.89	30.28	30.61	30.98	30.67	30.74	30.82	30.71	30.66	31.05	30.83	31.17	30.62	30.96
As_2O_5	0.00	0.00	0.00	0.00	0.00	0.00	0.00	0.00	0.00	0.00	0.00	0.00	0.00	0.00
SO_3	0.02	0.02	0.02	0.03	0.03	0.03	0.01	0.02	0.02	0.02	0.02	0.02	0.01	0.01
SiO_2	0.00	0.05	0.00	0.00	0.00	0.01	0.00	0.00	0.00	0.00	0.02	0.00	0.00	0.00
ThO_2	4.35	4.83	4.57	4.23	2.84	4.93	4.07	4.49	4.54	4.00	4.97	3.83	3.07	2.74
UO_2	0.49	0.38	0.62	0.50	0.40	0.48	0.51	0.57	0.58	0.49	0.49	0.36	0.35	0.37
Al_2O_3	0.00	0.00	0.00	0.00	0.00	0.00	0.00	0.00	0.00	0.00	0.00	0.00	0.00	0.00
Y_2O_3	2.02	1.79	2.39	2.14	1.67	1.89	1.75	2.25	2.20	1.89	1.79	1.65	1.62	1.75
La_2O_3	13.75	13.67	13.80	13.94	15.15	13.65	14.42	13.74	13.86	14.06	13.74	14.46	14.36	14.63
Ce_2O_3	28.28	27.62	27.64	28.26	29.33	27.36	28.89	28.23	28.01	28.51	27.88	29.04	29.30	28.85
Pr_2O_3	2.83	2.83	2.66	2.87	2.93	2.86	2.89	2.77	2.79	2.86	2.81	2.82	2.88	2.94
Nd_2O_3	12.43	12.24	11.88	12.68	12.70	12.38	12.43	12.08	12.38	12.46	12.41	12.28	13.03	12.98
Sm_2O_3	2.23	2.29	2.06	2.33	2.25	2.31	2.21	2.25	2.23	2.29	2.28	2.19	2.39	2.38
Eu_2O_3	0.26	0.22	0.22	0.25	0.16	0.26	0.26	0.19	0.17	0.27	0.23	0.26	0.28	0.19
Gd_2O_3	1.62	1.52	1.44	1.62	1.47	1.63	1.56	1.53	1.63	1.65	1.56	1.48	1.53	1.70
Tb_2O_3	0.21	0.24	0.23	0.30	0.21	0.23	0.24	0.26	0.22	0.21	0.21	0.25	0.24	0.26
Dy_2O_3	0.49	0.46	0.56	0.43	0.39	0.46	0.40	0.55	0.53	0.45	0.43	0.37	0.43	0.49
Ho_2O_3	0.03	0.03	0.03	0.04	0.05	0.07	0.01	0.03	0.02	0.06	0.03	0.00	0.07	0.03
Er_2O_3	0.48	0.53	0.46	0.42	0.43	0.45	0.43	0.49	0.42	0.41	0.45	0.40	0.43	0.39
Tm_2O_3	0.01	0.00	0.00	0.00	0.00	0.00	0.01	0.01	0.00	0.00	0.00	0.00	0.00	0.01
Yb_2O_3	0.00	0.00	0.00	0.02	0.00	0.00	0.00	0.00	0.00	0.00	0.02	0.00	0.00	0.00
Lu_2O_3	0.07	0.02	0.01	0.10	0.05	0.08	0.11	0.02	0.03	0.08	0.06	0.06	0.10	0.01
CaO	0.87	0.93	1.01	0.85	0.47	0.92	0.83	0.95	0.94	0.77	0.95	0.78	0.63	0.55
SrO	0.01	0.00	0.01	0.02	0.02	0.00	0.01	0.02	0.00	0.01	0.04	0.02	0.00	0.00
FeO	0.08	0.17	0.14	0.20	0.15	0.31	0.14	0.32	0.12	0.24	0.09	0.16	0.18	0.08
PbO	0.02	0.02	0.01	0.02	0.02	0.02	0.02	0.02	0.02	0.02	0.01	0.02	0.01	0.02
K_2O	0.01	0.01	0.01	0.02	0.01	0.92	0.83	0.95	0.94	0.77	0.95	0.78	0.63	0.55
Total	**101.46**	**100.15**	**100.40**	**102.25**	**101.40**	**101.10**	**102.05**	**101.54**	**101.35**	**101.82**	**101.30**	**101.62**	**101.55**	**101.35**
formulae based on 4 oxygen atoms														
P^{5+}	1.025	1.021	1.024	1.022	1.023	1.024	1.021	1.020	1.021	1.026	1.025	1.029	1.021	1.028
As^{5+}	0.000	0.000	0.000	0.000	0.000	0.000	0.000	0.000	0.000	0.000	0.000	0.000	0.000	0.000
S^{6+}	0.001	0.001	0.001	0.001	0.001	0.001	0.000	0.001	0.000	0.001	0.001	0.001	0.000	0.000
Si^{4+}	0.000	0.002	0.000	0.000	0.000	0.000	0.000	0.000	0.000	0.000	0.001	0.000	0.000	0.000
Th^{4+}	0.039	0.044	0.041	0.038	0.025	0.044	0.036	0.040	0.041	0.035	0.044	0.034	0.028	0.024
U^{4+}	0.004	0.003	0.005	0.004	0.004	0.004	0.004	0.005	0.005	0.004	0.004	0.003	0.003	0.003

Table 1 (continued)

Grain No.	**1**	**2**	**3**	**4**	**5**	**6**	**7**	**8**	**9**	**10**	**11**	**12**	**13**	**14**
An. No.	**1**	**2**	**1**	**1**	**3**	**1**	**1**	**1**	**3**	**1**	**1**	**1**	**2**	**2**
Al^{3+}	0.000	0.000	0.000	0.000	0.000	0.000	0.000	0.000	0.000	0.000	0.000	0.000	0.000	0.000
Y^{3+}	0.042	0.038	0.050	0.044	0.035	0.040	0.036	0.047	0.046	0.039	0.037	0.034	0.034	0.037
La^{3+}	0.199	0.201	0.201	0.200	0.220	0.198	0.208	0.199	0.201	0.202	0.199	0.208	0.209	0.212
Ce^{3+}	0.406	0.403	0.400	0.403	0.423	0.394	0.414	0.405	0.403	0.407	0.401	0.415	0.422	0.414
Pr^{3+}	0.040	0.041	0.038	0.041	0.042	0.041	0.041	0.040	0.040	0.041	0.040	0.040	0.041	0.042
Nd^{3+}	0.174	0.174	0.168	0.176	0.179	0.174	0.174	0.169	0.174	0.174	0.174	0.171	0.183	0.182
Sm^{3+}	0.030	0.031	0.028	0.031	0.031	0.031	0.030	0.030	0.030	0.031	0.031	0.029	0.032	0.032
Eu^{3+}	0.004	0.003	0.003	0.003	0.002	0.003	0.003	0.002	0.002	0.004	0.003	0.003	0.004	0.003
Gd^{3+}	0.021	0.020	0.019	0.021	0.019	0.021	0.020	0.020	0.021	0.021	0.020	0.019	0.020	0.022
Tb^{3+}	0.003	0.003	0.003	0.004	0.003	0.003	0.003	0.003	0.003	0.003	0.003	0.003	0.003	0.003
Dy^{3+}	0.006	0.006	0.007	0.005	0.005	0.006	0.005	0.007	0.007	0.006	0.005	0.005	0.005	0.006
Ho^{3+}	0.000	0.000	0.000	0.001	0.001	0.001	0.000	0.000	0.000	0.001	0.000	0.000	0.001	0.000
Er^{3+}	0.006	0.007	0.006	0.005	0.005	0.006	0.005	0.006	0.005	0.005	0.006	0.005	0.005	0.005
Yb^{3+}	0.000	0.000	0.000	0.000	0.000	0.000	0.000	0.000	0.000	0.000	0.000	0.000	0.000	0.000
Lu^{3+}	0.001	0.000	0.000	0.001	0.001	0.001	0.001	0.000	0.000	0.001	0.001	0.001	0.001	0.000
Ca^{2+}	0.036	0.039	0.043	0.035	0.020	0.039	0.035	0.040	0.040	0.032	0.040	0.033	0.027	0.023
Sr^{2+}	0.000	0.000	0.000	0.000	0.001	0.000	0.000	0.001	0.000	0.000	0.001	0.000	0.000	0.000
Fe^{2+}	0.003	0.006	0.005	0.006	0.005	0.010	0.004	0.011	0.004	0.008	0.003	0.005	0.006	0.003
K^{+}	0.001	0.000	0.001	0.001	0.001	0.001	0.001	0.002	0.001	0.001	0.001	0.001	0.001	0.000
Total	**2.041**	**2.045**	**2.044**	**2.044**	**2.043**	**2.044**	**2.045**	**2.049**	**2.045**	**2.042**	**2.040**	**2.040**	**2.047**	**2.040**
Position A	**1.015**	**1.021**	**1.019**	**1.022**	**1.020**	**1.018**	**1.023**	**1.028**	**1.024**	**1.015**	**1.014**	**1.010**	**1.025**	**1.012**
Position B	**1.026**	**1.024**	**1.025**	**1.023**	**1.023**	**1.025**	**1.022**	**1.021**	**1.021**	**1.027**	**1.027**	**1.030**	**1.021**	**1.028**
Σ LREE (apfu)	0.849	0.851	0.835	0.852	0.894	0.839	0.867	0.843	0.849	0.855	0.845	0.863	0.888	0.882
Σ HREE+Y (apfu)	0.079	0.074	0.085	0.082	0.068	0.077	0.072	0.084	0.083	0.076	0.073	0.067	0.070	0.074
X hut	0.000	0.185	0.000	0.000	0.000	0.028	0.000	0.000	0.000	0.000	0.074	0.000	0.000	0.000
X chrl	7.843	8.312	8.763	7.575	4.777	8.546	7.396	8.305	8.342	7.085	8.661	6.913	5.575	5.012
X mnz	92.157	91.503	91.237	92.425	95.223	91.425	92.604	91.695	91.658	92.915	91.265	93.087	94.425	94.988

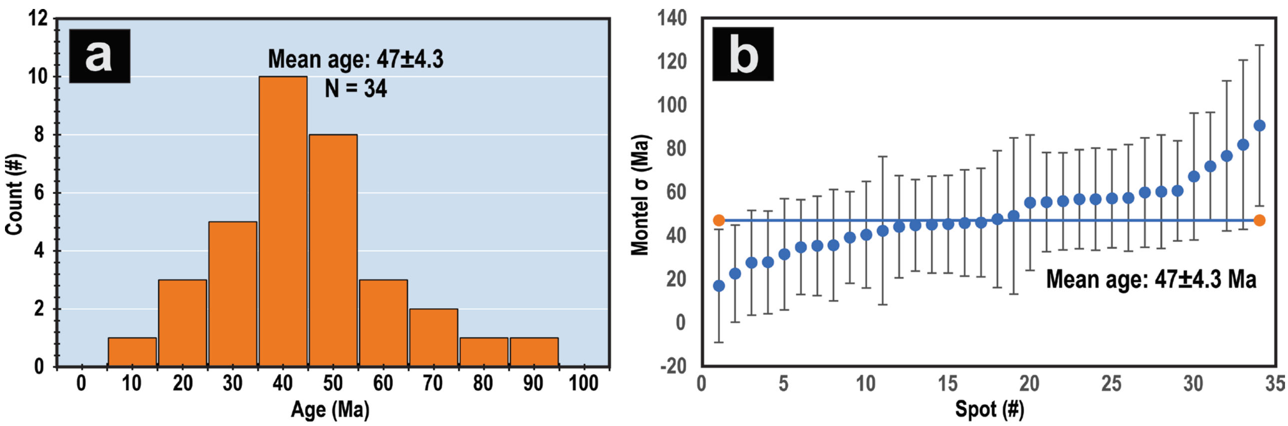

Fig. 4. a — Monazite age probability plot with histograms for sample RA–M–10. **b** — Diagram showing the single age sigma errors for monazite ages.

radiating fractures as the high concentration of uranium damages the crystal structure and makes it amorphous. The ^{238}U concentration is higher than ^{235}U concentration and therefore, the ^{238}U is easier to measure precisely (Hefferan & O'Brien 2010). The low concentration of ^{207}Pb will make it difficult for determining the apparent $^{207}Pb/^{235}U$ age as the data is less accurate and less precise (Hefferan & O'Brien 2010). Therefore in the current scenario, the $^{206}Pb/^{238}U$ Concordia dates were used for age calculation.

$^{206}Pb/^{238}U$ ages of sample RA–M–08 zircons typically ranging from 87.6 to 123.6 Ma (Fig. 5a, b, Table 3). A total of 46 zircon grains were analyzed for dating which produced a reliable consistent age of 103.1±2.9 Ma (Fig. 5a). The inherited zircon grains yielded age c. 460 Ma. Th/U ratio for

Table 2: U–Th–Pb geochronological data for all monazite analyses in sample RA–M–10.

An. No	Th [ppm]	U [ppm]	Th/U	Pb [ppm]	Y [ppm]	Th corr	U corr	Pb corr	Y corr	Th^2 σ	U^2 σ	Pb^2 σ	Age [Ma]	Montel σ [Ma]
mnz1-1	3.82	0.44	8.8	0.01	1.59	3.78	0.43	0.01	1.57	0.03	0.01	0.01	**40.40**	24.49
mnz1-2	3.73	0.37	10.1	0.01	1.37	3.69	0.36	0.01	1.36	0.03	0.01	0.01	**35.63**	25.55
mnz1-3	2.97	0.33	9.0	0.01	1.32	2.94	0.33	0.01	1.30	0.03	0.01	0.01	**55.15**	31.11
mnz1-4	2.84	0.30	9.4	0.01	1.34	2.81	0.30	0.00	1.33	0.03	0.01	0.01	**16.98**	25.97
mnz1-5	3.68	0.42	8.7	0.02	1.46	3.64	0.42	0.02	1.45	0.03	0.01	0.01	**71.80**	24.88
mnz1-6	3.78	0.52	7.2	0.02	1.78	3.74	0.52	0.01	1.76	0.03	0.01	0.01	**60.60**	22.97
mnz1-7	3.68	0.51	7.2	0.01	1.83	3.64	0.51	0.01	1.81	0.03	0.01	0.01	**27.78**	23.60
mnz2-1	4.05	0.60	6.8	0.02	1.80	4.01	0.59	0.01	1.78	0.03	0.01	0.01	**44.73**	21.05
mnz2-2	4.24	0.34	12.5	0.02	1.41	4.20	0.34	0.01	1.40	0.03	0.01	0.01	**44.09**	23.51
mnz2-3	3.76	0.42	9.0	0.02	1.48	3.73	0.42	0.01	1.46	0.03	0.01	0.01	**57.34**	24.52
mnz3-1	4.02	0.55	7.3	0.01	1.88	3.98	0.54	0.01	1.86	0.03	0.01	0.01	**34.72**	21.75
mnz3-2	3.75	0.50	7.5	0.02	1.73	3.71	0.49	0.01	1.72	0.03	0.01	0.01	**56.77**	23.45
mnz3-3	3.71	0.47	7.9	0.01	1.74	3.67	0.47	0.01	1.73	0.03	0.01	0.01	**27.56**	24.07
mnz4-1	3.72	0.44	8.4	0.02	1.69	3.68	0.44	0.01	1.67	0.03	0.01	0.01	**45.82**	24.41
mnz5-1	3.83	0.55	7.0	0.02	1.83	3.79	0.54	0.01	1.81	0.03	0.01	0.01	**55.41**	22.83
mnz5-2	1.86	0.42	4.4	0.02	1.36	1.84	0.42	0.01	1.35	0.02	0.01	0.01	**81.76**	38.87
mnz5-3	2.49	0.35	7.0	0.02	1.31	2.47	0.35	0.01	1.30	0.03	0.01	0.01	**76.70**	34.49
mnz6-1	4.34	0.42	10.3	0.02	1.49	4.29	0.42	0.01	1.48	0.03	0.01	0.01	**45.31**	22.47
mnz7-1	3.58	0.45	7.9	0.01	1.38	3.54	0.45	0.01	1.37	0.03	0.01	0.01	**46.00**	24.95
mnz8-1	3.95	0.50	7.8	0.02	1.77	3.91	0.50	0.01	1.76	0.03	0.01	0.01	**57.04**	22.53
mnz8-2	3.93	0.49	8.0	0.01	1.58	3.89	0.49	0.01	1.57	0.03	0.01	0.01	**35.33**	22.80
mnz8-3	3.80	0.35	10.9	0.01	1.45	3.76	0.34	0.01	1.44	0.03	0.01	0.01	**31.45**	25.54
mnz9-1	4.25	0.53	8.0	0.02	1.72	4.21	0.53	0.01	1.70	0.03	0.01	0.01	**39.14**	21.06
mnz9-2	3.69	0.40	9.2	0.02	1.38	3.65	0.40	0.01	1.37	0.03	0.01	0.01	**59.82**	25.16
mnz9-3	3.99	0.51	7.9	0.02	1.73	3.95	0.50	0.01	1.72	0.03	0.01	0.01	**45.12**	22.32
mnz9-4	4.38	0.38	11.5	0.02	1.31	4.33	0.38	0.01	1.30	0.03	0.01	0.01	**55.82**	22.36
mnz10-1	3.51	0.43	8.1	0.02	1.49	3.48	0.43	0.01	1.47	0.03	0.01	0.01	**60.17**	26.03
mnz11-1	4.37	0.43	10.2	0.01	1.41	4.32	0.42	0.01	1.39	0.04	0.01	0.01	**22.61**	22.29
mnz11-2	4.22	0.40	10.5	0.02	1.43	4.18	0.40	0.01	1.41	0.03	0.01	0.01	**56.70**	22.76
mnz12-1	3.36	0.31	10.7	0.02	1.30	3.33	0.31	0.01	1.29	0.03	0.01	0.01	**67.17**	29.17
mnz13-1	2.89	0.34	8.4	0.01	1.32	2.86	0.34	0.01	1.31	0.03	0.01	0.01	**47.65**	31.44
mnz13-2	2.70	0.31	8.7	0.01	1.28	2.67	0.31	0.01	1.26	0.03	0.01	0.01	**42.26**	34.01
mnz14-1	2.48	0.31	7.9	0.01	1.38	2.46	0.31	0.01	1.37	0.03	0.01	0.01	**49.08**	35.93
mnz14-2	2.41	0.32	7.4	0.02	1.38	2.38	0.32	0.01	1.37	0.03	0.01	0.01	**90.62**	36.93

the sample ranges up to 0.4, with most values arround 0.2 typical for metamorphic zircons (Table 3). Similarly, a total 8 analyses are obtained from zircon grains in sample RA–M–41 ranging in age from 98.6 to 764.9 Ma ($^{206}Pb/^{238}U$) and 87.9 to 825.9 Ma ($^{207}Pb/^{206}Pb$; Fig. 5c, d, Table 3). Intersect age diagram provides age 100.0±5.3 Ma (Fig. 5c). The divergence between the two data sets is accompanied by a significant discordance in both the Wetherill and Tera–Wasserburg diagrams (Fig. 5a–d). The inherited zircon grains yielded discordant ages with apparent ages ranging from c. 566 to 765 Ma (Fig. 5d). These inherited zircons may be acquired from the nearby country rocks or may have either been derived from the source rocks itself. Th/U ration for young ages ranges up to 0.2 pointing out the metamorphic origin. Inherited ages provide higher Th/U ratio between 0.5 to 0.9 (Table 3).

Tera Wasserburg Intersect ages ($^{238}U/^{206}Pb$) generated for the two samples are within the analytical error of one another: 103.1±2.9 Ma (sample RA–M–08) and 100.0±5.3 Ma (sample RA–M–41).

Discussion

The new U–Pb age data presented in this paper are plotted on Figure 5a–f, together with U–Th–Pb data from southern KMC, Hunza region. In the southern KMC, Hunza region of the Asian Plate margin Searle & Tirrul (1991) and Fraser et al. (2001) have defined the metamorphism and deformation in D1, M0 and M1 (M1–a, M1–b and M1–c) from Late Cretaceous–Early Paleocene to Late Eocene–Oligocene in the result of accretion of the Kohistan Arc to the southern margin of Asia and then India–Asia collision. Searle & Tirrul (1991) suggested the early subduction related metamorphism in the Hunza Valley as contact metamorphism and termed as M1 like in Baltoro region, but Fraser et al. (2001) define as M0 for both the Hunza Valley and Baltoro region. Based on the dating of sample K98-6P by Fraser et al. (2001), they concluded the early stages of metamorphism in Hunza Valley occurred more than 60 Ma ago in contrast of Searle & Tirrul (1991) as they suggested the high–grade metamorphism along the southern

Table 3: U–Pb geochronological data for zircon grains in samples RA–M–08 and RA–M–41.

RA–M–08 An. No.	Th [ppm]	U [ppm]	Th/U	$^{207}Pb/^{235}U$	±σ [%]	$^{206}Pb/^{238}U$	±σ [%]	ρ	$^{207}Pb/^{206}U$ Age [Ma]	±2σ [Ma]	$^{207}Pb/^{235}U$ Age [Ma]	±2σ [Ma]	$^{206}Pb/^{238}U$ Age [Ma]	±2σ [Ma]	Disc. [%]
01a	3.2	18.8	0.2	0.0933	4.44	0.0137	2.62	0.59	171.4	171.4	90.6	7.7	87.6	4.6	3.31
01b	6.7	25.6	0.3	0.1102	2.92	0.0166	1.60	0.55	106.8	106.8	106.2	5.9	106.2	3.4	–0.02
01c	6.2	24.9	0.2	0.1064	3.24	0.0162	1.79	0.55	89.5	89.5	102.7	6.3	103.3	3.7	–0.60
02a	2.5	32.0	0.1	0.0987	2.45	0.0153	1.40	0.57	41.2	41.2	95.6	4.5	97.8	2.7	–2.34
02b	3.6	27.8	0.1	0.1025	2.42	0.0165	1.60	0.66	–58.8	–58.8	99.0	4.6	105.8	3.4	–6.79
03a	4.2	13.1	0.3	0.1330	3.38	0.0188	2.28	0.67	251.5	251.5	126.8	8.0	120.3	5.4	5.13
03b	4.4	14.1	0.3	0.1267	2.97	0.0188	1.85	0.62	140.9	140.9	121.1	6.8	120.2	4.4	0.79
04a	12.6	40.3	0.3	0.1193	2.16	0.0177	1.52	0.70	141.6	141.6	114.4	4.7	113.2	3.4	1.09
04b	22.0	58.7	0.4	0.1128	2.05	0.0166	1.47	0.72	159.5	159.5	108.6	4.2	106.3	3.1	2.08
05	9.1	33.1	0.3	0.1088	2.46	0.0166	1.43	0.58	76.3	76.3	104.9	4.9	106.2	3.0	–1.25
06	1.2	15.6	0.1	0.1321	4.82	0.0182	2.22	0.46	309.3	309.3	126.0	11.4	116.5	5.1	7.51
07a	5.6	25.3	0.2	0.1285	2.62	0.0183	1.81	0.69	238.7	238.7	122.7	6.0	116.9	4.2	4.77
07b	2.1	12.2	0.2	0.1549	3.25	0.0181	1.94	0.60	675.5	675.5	146.2	8.8	115.7	4.5	20.85
08	7.7	31.8	0.2	0.1094	2.95	0.0163	2.03	0.69	139.2	139.2	105.4	5.9	104.0	4.2	1.37
09a	3.0	23.1	0.1	0.1213	3.43	0.0177	2.12	0.62	176.7	176.7	116.2	7.5	113.3	4.8	2.48
09b	2.9	17.8	0.2	0.1033	3.44	0.0162	2.04	0.59	4.6	4.6	99.8	6.5	103.9	4.2	–4.08
10a	2.3	103.6	0.0	0.0915	4.29	0.0141	2.49	0.58	44.2	44.2	88.9	7.3	90.6	4.5	–1.92
10b	2.3	56.7	0.0	0.0985	4.79	0.0153	2.69	0.56	41.7	41.7	95.4	8.7	97.6	5.2	–2.31
10c	1.5	57.0	0.0	0.0988	4.62	0.0140	2.92	0.63	248.9	248.9	95.6	8.4	89.7	5.2	6.27
11a	4.6	27.8	0.2	0.1295	2.78	0.0188	1.90	0.68	190.3	190.3	123.7	6.5	120.3	4.5	2.74
11b	9.6	57.7	0.2	0.1027	2.38	0.0154	1.64	0.69	120.8	120.8	99.2	4.5	98.4	3.2	0.86
12	5.6	190.3	0.0	0.5970	1.68	0.0740	1.45	0.86	549.8	549.8	475.3	12.7	460.2	12.8	3.18
13a	2.5	14.3	0.2	0.1103	3.32	0.0169	1.77	0.53	64.3	64.3	106.3	6.7	108.2	3.8	–1.82
13b	4.2	20.5	0.2	0.1072	5.43	0.0156	2.86	0.53	180.3	180.3	103.4	10.6	100.1	5.7	3.16
14a	4.5	28.1	0.2	0.1054	3.97	0.0151	2.13	0.54	228.4	228.4	101.7	7.6	96.4	4.1	5.19
14b	12.2	39.0	0.3	0.1186	2.81	0.0177	2.09	0.74	134.7	134.7	113.8	6.0	112.8	4.7	0.83
15	10.3	34.9	0.3	0.1066	2.87	0.0153	1.76	0.61	228.2	228.2	102.9	5.6	97.6	3.4	5.14
16a	5.2	31.6	0.2	0.1007	3.76	0.0151	2.00	0.53	116.0	116.0	97.5	7.0	96.8	3.8	0.73
16b	5.4	30.2	0.2	0.0964	3.19	0.0156	1.97	0.62	–65.6	–65.6	93.4	5.7	99.8	3.9	–6.83
17	11.6	26.2	0.4	0.1059	2.84	0.0163	1.69	0.60	63.3	63.3	102.2	5.5	104.0	3.5	–1.69
18	15.3	158.2	0.1	0.1050	2.83	0.0158	1.93	0.68	112.6	112.6	101.4	5.4	101.0	3.9	0.42
19a	2.3	291.7	0.0	0.0938	2.22	0.0144	1.75	0.79	66.7	66.7	91.1	3.9	92.1	3.2	–1.07
19b	2.0	254.3	0.0	0.0970	2.05	0.0143	1.57	0.77	152.8	152.8	94.0	3.7	91.7	2.9	2.41
20	4.2	27.5	0.2	0.1245	3.52	0.0157	1.95	0.55	518.7	518.7	119.2	7.9	100.2	3.9	15.96
21	8.8	43.6	0.2	0.1123	2.16	0.0162	1.49	0.69	205.8	205.8	108.0	4.4	103.7	3.1	4.02
22a	20.9	54.3	0.4	0.1082	2.43	0.0168	1.66	0.68	34.0	34.0	104.3	4.8	107.5	3.5	–3.02
22b	31.2	72.1	0.4	0.1122	1.91	0.0167	1.29	0.67	133.6	133.6	108.0	3.9	106.8	2.7	1.03
23	4.3	36.9	0.1	0.1326	2.24	0.0194	1.65	0.73	181.0	181.0	126.4	5.3	123.6	4.0	2.24
24	3.0	12.5	0.2	0.1088	3.50	0.0167	1.89	0.54	55.8	55.8	104.9	6.9	107.1	4.0	–2.12
25a	3.3	34.3	0.1	0.1065	4.39	0.0157	2.14	0.49	159.4	159.4	102.7	8.5	100.4	4.3	2.32
25b	2.6	54.5	0.0	0.1059	3.42	0.0149	2.22	0.65	258.8	258.8	102.2	6.6	95.6	4.2	6.41
26	4.1	21.0	0.2	0.1115	3.01	0.0162	1.65	0.55	189.7	189.7	107.3	6.1	103.7	3.4	3.38
27	22.1	123.8	0.2	0.1139	2.08	0.0166	1.55	0.75	188.7	188.7	109.5	4.3	106.0	3.2	3.25
28a	3.5	20.7	0.2	0.1114	3.39	0.0168	2.32	0.68	108.0	108.0	107.3	6.9	107.3	4.9	–0.02
28b	2.6	21.4	0.1	0.1255	3.56	0.0179	2.09	0.59	233.5	233.5	120.0	8.0	114.4	4.7	4.66
29	6.3	38.9	0.2	0.1037	2.65	0.0151	1.55	0.58	191.7	191.7	100.2	5.0	96.5	3.0	3.75
RA–M–41 An. No.	**Th [ppm]**	**U [ppm]**	**Th/U**	**$^{207}Pb/^{235}U$**	**±σ [%]**	**$^{206}Pb/^{238}U$**	**±σ [%]**	**ρ**	**$^{207}Pb/^{206}U$ Age [Ma]**	**±2σ [Ma]**	**$^{207}Pb/^{235}U$ Age [Ma]**	**±2σ [Ma]**	**$^{206}Pb/^{238}U$ Age [Ma]**	**±σ [Ma]**	**Disc. [%]**
01a	2.9	19.4	0.1	0.1015	3.69	0.0154	2.39	0.65	87.9	133.3	98.1	6.9	98.6	4.7	–0.48
01b	12.2	74.6	0.2	0.1144	2.23	0.0162	1.46	0.66	245.6	77.7	110.0	4.6	103.9	3.0	5.56
01c	7.1	24.8	0.3	0.1078	2.56	0.0171	1.68	0.66	–14.7	92.9	104.0	5.0	109.3	3.6	–5.09
01d	6.9	25.2	0.3	0.1106	2.60	0.0163	1.46	0.56	156.3	100.8	106.5	5.2	104.3	3.0	2.04
02a	3.5	11.2	0.3	0.9926	2.38	0.1081	2.05	0.86	825.9	49.9	700.0	23.8	661.7	25.8	5.47
02b	4.4	10.0	0.4	1.1319	2.21	0.1260	1.95	0.88	780.7	43.8	768.7	23.6	764.9	28.1	0.50
03a	2.8	24.4	0.1	0.8360	2.72	0.0918	2.36	0.87	808.7	57.1	617.0	24.9	566.2	25.5	8.22
03b	2.8	24.4	0.1	0.9192	2.55	0.1052	2.08	0.82	721.9	62.7	661.9	24.5	644.7	25.5	2.60

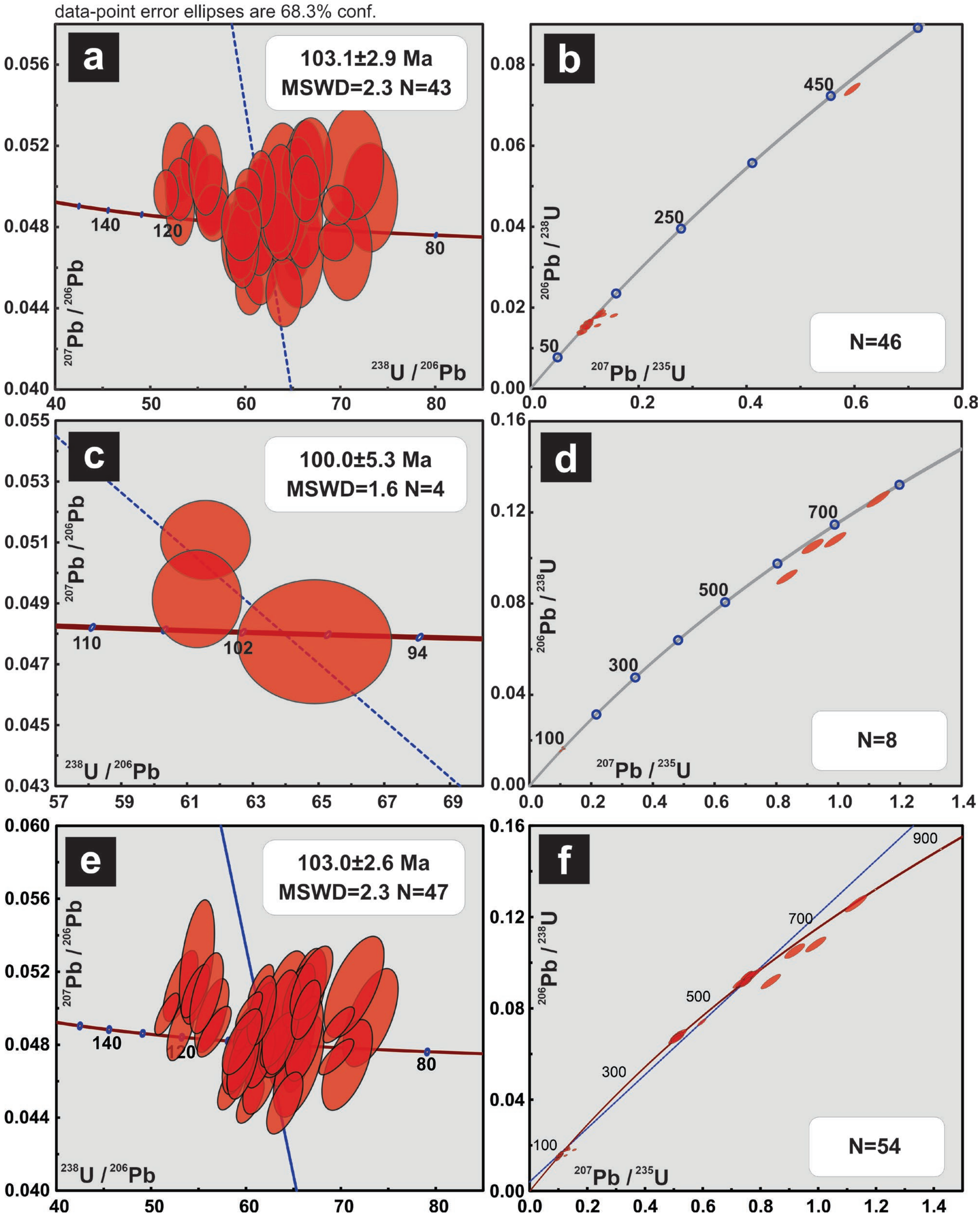

Fig. 5. U–Pb diagrams. **a** — Tera–Wasserburg diagram showing zircon intersect ages from sample RA–M–08. **b** — Conventional Wetherill concordia plot showing all zircon ages from sample RA–M–08. **c** — Tera–Wasserburg diagram showing zircon intersect ages from sample RA–M–41. **d** — Conventional Wetherill concordia plot showing all zircon ages from sample RA–M–41. **e, f** — Combined Tera–Wasserburg and Wetherill concordia plot for samples RA–M–08 and RA–M–41. The plots were produced using the Isoplot program (Ludwig 2011).

Karakoram occurred after the India–Asia collision i.e. 54–50 Ma. In result, Fraser et al. (2001) define this metamorphism as M1–a in the Hunza Valley as a result of collision between the Kohistan Island Arc and southern Asian Plate margin during the Late Cretaceous. Similarly, the related deformation was named as D1 in the result of closure across the Shyok Suture Zone (Fig. 1). In addition, the peaked sillimanite grade metamorphism in the Hunza Valley is termed as M1–b influenced by the consequent accretion of India to Asia. The youngest episode of continuous crustal thickening related to India–Asia collision is termed as M1–c in the form of later sillimanite grade metamorphism (U–Pb monazite; 44.0±2.0; Fraser et al. 2001).

The Hunza Plutonic Unit of Karakoram Batholith resulted from the subduction of the Tethys Ocean beneath the southern Asian margin during the Cretaceous experiences the crystallization ages ranging between c. 105 and c. 95 Ma (Palin et al. 2012). There is no such geochronological evidence reported in the Hunza Valley in the west and Baltoro region in the east (fig. 1 in Palin et al. 2012) due to complex tectonic setting and polymetamoprhic history of southern KMC of the Asian Plate margin. The polymetamorphic characteristics lead to recrystallizing the original monazite within high-grade units of multiply deformed rocks. Notably, garnet can serve as a protective shield for monazite, preventing the alteration of its composition even in temperatures exceeding 850 °C (Montel et al. 2000). The geochronological interpretations of samples RA–M–08 and RA–M–41 for zircon analyses suggest the pre India–Asia collision and produce the U–Pb ages of 103.1±2.9 Ma and 100.0±5.3 Ma Ma respectively (Fig. 5a, c). This period may be linked to peri-plutonic thermal metamorphism tied to the development of the axial Karakoram Batholith. Similar ages might thus be retained in various other rocks distributed throughout the Karakoram Range that were in close vicinity near subduction–associated components of the Karakoram Batholith (Palin et al. 2012).

Well exposed metamorphic stacks in the Hunza Valley exhibit a general trend of increasing age and peak pressure–temperature conditions toward north. These units have been located alongside one another through a series of east–west trending thrust faults (Fraser 2000; Fraser et al. 2001). Metamorphic P–T–t information for specific tectonostratigraphic units (kyanite- and garnet–chloritoid-grade) is presently lacking, and the chronology of movements along certain bounding faults remains somewhat uncertain (see Palin et al. 2012 for detail). With the acquisition of new U–Pb age data regarding the sillimanite–grade, sillimanite–kyanite–grade and staurolite grade overprinting of pelitic rocks, we can impose strict constraints on the timing of metamorphism in the garnet–chloritoid-grade units.

The emplacement of Hunza Plutonic Unit on the upper sillimanite zone metamorphic suits (Palin et al. 2012) by Hunza Thrust is well constrained by set 1 and set 2 Hunza dykes intrusion. Set 1 dykes documented with U–Pb zircon crystallization ages of 52–50 Ma (Fraser et al. 2001) intruded the Hunza Plutonic Unit rocks and are reported with deformation along the Hunza Thrust in the southward direction. The younger set 2 dykes (U–Pb zircon; 35.0±1.0 Ma) passed through the tectonic fabrics in both the Hunza Plutonic Unit and upper sillimanite zone (Fraser et al. 2001). This strongly give the evidence for the final motion along the Hunza Thrust between c. 50 and c. 35 Ma in the Hunza region in the southern KMC of the Asian Plate margin that is consistent with our monazite age of 47±4.3 Ma.

Further south, staurolite-grade metamorphic units dated 16.0±1.0 Ma (U–Pb monazite; Fraser et al. 2001) are exposed in the Hunza region which are overthrusted by kyanite-grade units along the North Murtzabad Thrust (see fig. 11 for details in Palin et al. 2012). Similarly, the lower sillimanite zone units separate these kyanite-grade units along the Hassanabad Thrust Fault. According to Fraser et al. (2001), metamorphism occurred at 44.0±2.0 Ma (U–Pb monazite) and data from our sample RA–M–10 (U–Pb monazite; 47±4.3 Ma) may show peak sillimanite grade metamorphism within the region.

Further south, younger kyanite–grade metamorphism is reported as 28.2±0.8 Ma. All data show the relative timing of metamorphism and structural movements within the Hunza region along the southern margin of Asian Plate margin. Similarly the emplacement of post collisional Miocene S–type Sumayar Granite (Hussain et al. 2024) at 9.3±0.1 Ma (U–Pb uraninite; Fraser et al. 2001) separates the staurolite and kyanite-grade units and shows the thermal metamorphism within the country rocks (Crawford & Searle 1993). Overall these data agree to conclude that the final peak metamorphism in the Hunza region occurred between c. 16 and c. 9 Ma. The data broadly support the chronology of metamorphism and deformation events proposed by Searle (1991), Searle & Tirrul (1991), Fraser et al. (2001), and Palin et al. (2012).

The Cretaceous collision metamorphic event in the Karakoram tectonic unit, related to subduction of the Tethys Ocean beneath the southern Asian margin, can be timely correlated with the subduction and closure of the southern Alpine (Piemont–Liguria) Tethys in the Alps. Similarly, the Eocene India–Asia collision and the final Tethys closure is contemporaneous with the northern Alpine (Valais) Tethys subduction and Adria–Eurasia collision event (e.g., Schmid et al. 2008). Cretaceous collision metamorphic event was detected in the Inner (Central) Western Carpathians with the Austroalpine affinity (Plašienka et al. 1997), whereas the Eocene tectonometamorphic event was constrained in the Inner Western Carpathians orogenic front Infratatric Unit (Putiš et al. 2021).

Conclusions

U–Pb zircon ages of 103.1±2.9 Ma and 100.0±5.3 Ma obtained from samples RA–M–08 (Grt–Cpx–Hbd orthogeniss) and RA–M–41 (metapelitic schist), respectively from the KMC in Hunza Valley reveals sillimanite–kyanite grade and staurolite grade peri-plutonic thermal metamorphism related to the Tethyan Ocean subduction that resulted in the formation of the Cretaceous Hunza Plutonic Unit of the Karakoram Batholith.

U–Pb monazite age of 47±4.3 Ma from sample RA–M–10 (pelitic schist) shows the peak sillimanite grade metamorphism and continued further after its initial collision, followed by the later India–Asia collision.

This suggests that the earliest metamorphic event is related to collision of the Kohistan Island Arc with the Asian Plate, whereas the later India–Asia collision is represented by a new increment of crustal thickening-related deformation, metamorphism and magmatism in the region.

Acknowledgements: This research is part of the PhD work of the first author. The authors acknowledge the Higher Education Commission (HEC) of Pakistan and Slovak Academic Information Agency (SAIA) Slovakia for funding of his stays at the Oxford University, United Kingdom and Comenius University in Bratislava respectively. Funded by the EU NextGenerationEU through the Recovery and Resilience Plan for Slovakia under the project No. 09I03-03-V04-00071. The suggestions of two reviewers contributed to the significant improvement of the original manuscript and are appreciated very much.

References

Allen T. & Chamberlain P.C. 1991: Metamorphic evidence for an inverted crustal section, with constraints on the Main Karakoram thrust, Baltistan, northern Pakistan. *Journal of Metamorphic Geology* 9, 403–418. https://doi.org/10.1111/j.1525-1314.1991.tb00535.x

Bertrand J.M., Kienast J.R. & Pinardon J.L. 1988: Structure and metamorphism of the Karakoram gneisses in the Braldu–Baltoro Valley (North Pakistan). *Geodinamica Acta* 2, 135–150. https://doi.org/10.1080/09853111.1988.11105162

Black L.P., Kamo S.L., Allen C.M., Davis D.W. Aleinikoff, J.N. Valley, J.W. Mundil, R., Campbell I.H., Korsch R.J., Williams I.S. & Foudoulis C. 2004: Improved $^{206}Pb/^{238}U$ microprobe geochronology by the monitoring of a trace–element–related matrix effect; SHRIMP, ID–TIMS, ELA–ICP–MS and oxygen isotope documentation for a series of zircon standards. *Chemical Geology* 205, 115–140. https://doi.org/10.1016/j.chemgeo.2004.01.003

Brandon C. & Romanowicz B. 1986: A "No-Lid" zone in the Central Chang-Thang platform of Tibet: evidence from pure path phase velocity measurements of long period Rayleigh waves. *Journal of Geophysical Research* 91, 6547–6564. https://doi.org/10.1029/JB091iB06p06547

Caporali A. 2000: The gravity field of the Karakoram Mountain Range and surrounding areas. *Geological Society, London, Special Publications* 170, 7–23. https://doi.org/10.1144/GSL.SP.2000.170.01.02

Carson C.J., Berman R.G., Stern R.A., Sanborn–Barrie M., Skulski T. & Sandeman H.A.I. 2004: Age constraints on the Paleoproterozoic tectonometamorphic history of the Committee Bay region, western Churchill Province, Canada: evidence from zircon and in situ monazite SHRIMP geochronology. *Canadian Journal of Earth Sciences* 41, 1049–1076. https://doi.org/10.1139/e04-05

Chen W.P. & Molnar P. 1983: Focal depths of intracontinental and intraplate earthquakes and their implications for the thermal and mechanical properties of the lithosphere. *Journal of Geophysical Research* 88, 4183–4214. https://doi.org/10.1029/JB088iB05p04183

Cherniak D.J., Watson E.B. & Grove M. 2004: Pb diffusion in monazite: a combined RBS/SIMS study. *Geochimica et Cosmochimica Acta* 68, 829–840. https://doi.org/10.1016/j.gca.2003.07.012

Corrie S.L. & Kohn M.J. 2008: Trace–element distributions in silicates during prograde metamorphic reactions: implications for monazite formation. *Journal of Metamorphic Geology* 26, 451–464. https://doi.org/10.1111/j.1525-1314.2008.00769.x

Crawford M.B. & Searle M.P. 1992: Field relationships and geochemistry of pre-collisional (India–Asia) granitoid magmatism in the central Karakoram. *Tectonophysics* 206, 171–192. https://doi.org/10.1016/0040-1951(92)90375-G

Crawford M.B. & Searle M.P. 1993: Collision–related granitoid magmatism and crustal structure of the Hunza Karakoram, north Pakistan. *Geological Society London, Special Publications* 74, 53–68. https://doi.org/10.1144/GSL.SP.1993.074.01.05

De Sigoyer J., Chavagnac V., Blichert–Toft J., Villa I.M., Luais B., Guillot S., Cosca M. & Mascle G. 2000: Dating the Indian continental subduction and collisional thickening in the northwest Himalaya: multichronology of the Tso Morari eclogites. *Geology* 28, 487–490.

Debon F. & Khan N.A. 1996: Alkaline orogenic plutonism in the Karakoram batholith: the Upper Cretaceous Koz Sar complex (Karamber valley, N. Pakistan). *Geodinamica Acta* 9, 145–160. https://doi.org/10.1080/09853111.1996.11105282

Debon F., Le Fort P., Dautel D., Sonet J. & Zimmermann J.L. 1987: Granites of western Karakoram and northern Kohistan (Pakistan): a composite mid–Cretaceous to upper Cenozoic magmatism. *Lithos* 20, 19–40. https://doi.org/10.1016/0024-4937(87)90022-3

Faisal S., Larson K.P., Cottle J.M. & Lamming J. 2014: Building the Hindu Kush: Monazite records of terrane accretion, plutonism and the evolution of the Himalaya–Karakoram–Tibet orogen. *Terra Nova* 26, 395–401. https://doi.org/10.1111/ter.12112

Foster G.L., Kinny P., Vance D., Prince C. & Harris N.B. 2000: The significance of monazite U–Th–Pb age data in metamorphic assemblages; a combined study of monazite and garnet chronometry. *Earth and Planetary Sciences Letters* 181, 327–340. https://doi.org/10.1016/S0012-821X(00)00212-0

Foster G.L., Gibson H.D., Parrish R.R., Horstwood M.S.A., Fraser J.E. & Tindle A. 2002: Textural, chemical and isotopic insights into the nature and behavior of metamorphic monazite. *Chemical Geology* 191, 183–207. https://doi.org/10.1016/S0009-2541(02)00156-0

Foster G., Parrish R.R., Horstwood M.S.A., Chenery S., Pyle J. & Gibson H.D. 2004: The generation of prograde P–T–t points and paths; a textural, compositional and chronological study of metamorphic monazite. *Earth and Planetary Science Letters* 228, 125–142. https://doi.org/10.1016/j.epsl.2004.09.024

Fraser J.E. 2000: The Structural and Metamorphic Evolution of the Deep Crust in the Hunza Karakoram, Pakistan. *PhD thesis, University of Oxford.*

Fraser J.E., Searle M.P, Parrish R.R. & Noble S.R. 2001: Chronology of deformation, metamorphism, and magmatism in the southern Karakoram Mountains. *Geological Society of America Bulletin* 113, 1443–1455. https://doi.org/10.1130/0016-7606(2001)113<1443:CODMAM>2.0.CO;2

Gaetani M. 1997: The Karakorum block in central Asia, from Ordovician to Cretaceous. *Sedimentary Geology* 109 339–359. https://doi.org/10.1016/S0037-0738(96)00068-1

Green O.R., Searle M.P., Corfield R.I. & Corfield R.M. 2008: Cretaceous–Tertiary carbonate platform evolution and the age of the India–Asia collision along the Ladakh Himalaya (Northwest India). *Journal of Geology* 116, 331–353. https://doi.org/10.1086/588831

Hawkins D.P., & Bowring S.A. 1999: U–Pb monazite, xenotime and titanite geochronological constraints on the prograde to post–peak metamorphic thermal history of Palaeoproterozoic migmatites from the Grand Canyon, Arizona. *Contributions to Mineralogy and Petrology* 134, 150–169. https://doi.org/10.1007/s004100050475

Hefferan K. & O'Brien J. 2010: Earth Materials. *John Wiley & Sons Ltd, Wiley–Blackwell*, UK

Hildebrand P.R., Noble S.R., Searle M.P., Parrish R.R. & Shakirullah 1998: Tectonic significance of 24 Ma crustal melting in the eastern Hindu Kush, Pakistan: *Geology* 26, 871–874. https://doi.org/10.1130/0091-7613(1998)026<0871:TSOMCM>2.3.CO;2

Hildebrand P.R., Searle M.P., Shakirullah, Khan Z. & Van Heijst H.J. 2000: Geological evolution of the Hindu Kush, NW Pakistan: Active margin to continent-continent collision zone, in Khan, M.A., et al., eds., Tectonics of the Nanga Parbat syntaxis and the western Himalaya: *Geological Society London Special Publication* 170, 277–293. https://doi.org/10.1144/GSL.SP.2000.170.01.15

Hildebrand P.R., Noble S.R., Searle M.P., Waters D.J. & Parrish, R.R. 2001: Old origin for an active mountain range: Geology and geochronology of the eastern Hindu Kush, Pakistan. *Geological Society of America Bulletin* 113, 625–639. https://doi.org/10.1130/0016-7606(2001)113<0625:OOFAAM>2.0.CO;2

Horstwood M.S., Košler J., Gehrels G., Jackson S.E., McLean N.M., Paton C., Pearson N.J., Sircombe K., Sylvester P., Vermeesch P. & Bowring J.F. 2016: Community–derived standards for LA–ICP–MS U–(Th–) Pb geochronology–Uncertainty propagation, age interpretation and data reporting. *Geostandards and Geoanalytical Research* 40, 311–332. https://doi.org/10.1111/j.1751-908X.2016.00379.x

Hussain A., Zhao K.D., Rehman H.U., Sadiq I., Li Q., Baig S.S. & Ullah I. 2024: Geochronology and petrogenesis of the Miocene S–type Sumayar granite in the Karakoram Block, north Pakistan: Implications for post–collisional magmatism. *Journal of Asian Earth Sciences* 264, 106053. https://doi.org/10.1016/j.jseaes.2024.106053

Janots E., Engi M., Berger A., Allaz J., Schwarz J.O. & Spandler C. 2008: Prograde metamorphic sequence of REE minerals in pelitic rocks of the Central Alps: implications for allanite–monazite–xenotime phase relations from 250 to 610 °C. *Journal of Metamorphic Geology* 26, 509–526. https://doi.org/10.1111/j.1525-1314.2008.00774.x

Kohn M.J. & Malloy M.A. 2004: Formation of monazite via prograde metamorphic reactions among common silicates: implications for age determinations. *Geochimica et Cosmochimica Acta* 68, 101–113. https://doi.org/10.1016/S0016-7037(03)00258-8

Kohn M.J., Wieland M.S., Parkinson C.D. & Upreti B.N. 2005: Five generations of monazite in Langtang gneisses: implications for chronology of the Himalayan metamorphic core. *Journal of Metamorphic Geology* 23, 399–406. https://doi.org/10.1111/j.1525-1314.2005.00584.x

Konečný P., Kusiak M.A. & Dunkley D.J. 2018: Improving U–Th–Pb electron microprobe dating using monazite age references. *Chemical Geology* 484, 22–35. https://doi.org/10.1016/j.chemgeo.2018.02.014

Larson K.P., Cottle J.M. & Godin L. 2011: Petrochronologic record of metamorphism and melting in the upper Greater Himalayan sequence, Manaslu–Himal Chuli Himalaya, west–central Nepal. *Lithosphere* 3, 379–392. https://doi.org/10.1130/L149.1

Larson K.P., Ali A., Shrestha S., Soret M., Cottle J.M. & Ahmad R. 2019: Timing of metamorphism and deformation in the Swat valley, northern Pakistan: Insight into garnet–monazite HREE partitioning. *Geoscience Frontiers* 10, 849–861. https://doi.org/10.1016/j.gsf.2018.02.008

Lemennicier Y., Le Fort P., Lombardo B., Pêcher A. & Rolfo F. 1996: Tectonometamorphic evolution of the central Karakorum (Baltistan–northern Pakistan). *Tectonophysics* 260, 119–143. https://doi.org/10.1016/0040-1951(96)00080-7

Ludwig K.R. 2011: Isoplot: A Plotting and Regression Program for Radiogenic Isotope Data. Version 4.13–March 2011. *US Geological Survey Open–File Report*, 1–445.

Mahar M.A., Mahéo G., Goodell P.C. & Pavlis T.L. 2014: Age and origin of post collision Baltoro granites, south Karakoram, North Pakistan: Insights from in–situ U–Pb, Hf and oxygen isotopic record of zircons. *Lithos* 205, 341–358. https://doi.org/10.1016/j.lithos.2014.07.014

Mahéo G., Bertrand H., Guillot S., Villa I.M., Keller F. & Capiez P. 2004: The South Ladakh ophiolites (NW Himalaya, India): an intra–oceanic tholeiitic arc origin with implication for the closure of the Neo–Tethys. *Chemical Geology* 203, 273–303. https://doi.org/10.1016/j.chemgeo.2003.10.007

Montel J.M., Kornprobst J. & Vielzeuf D. 2000: Preservation of old U–Th–Pb ages in shielded monazite: example from the Beni Bousera Hercynian kinzingites (Morocco). *Journal of Metamorphic Geology* 18, 335–342. https://doi.org/10.1046/j.1525-1314.2000.00261.x

Palin R., Searle M., Waters D., Horstwood M. & Parrish R. 2012: Combined thermobarometry and geochronology of peraluminous metapelites from the Karakoram metamorphic complex, North Pakistan; new insight into the tectonothermal evolution of the Baltoro and Hunza Valley regions. *Journal of Metamorphic Geology* 30, 793–820. https://doi.org/10.1111/j.1525-1314.2012.00999.x

Palin R.M., St-Onge M.R., Waters D.J., Searle M.P. & Dyck B. 2014: Phase equilibria modelling of retrograde amphibole and clinozoisite in mafic eclogite from the Tso Morari massif, northwest India: constraining the P–T–M(H2O). *Journal of Metamorphic Geology* 32, 675–693. https://doi.org/10.1111/jmg.12085

Parrish R.R. 1990: U–Pb dating of monazite and its application to geological problems. *Canadian Journal of Earth Sciences* 27, 1431–1450. https://doi.org/10.1139/e90-152

Parrish R.R. & Tirrul R. 1989: U–Pb age of the Baltoro granite, northwest Himalaya, and implications for zircon inheritance and monazite U–Pb systematics. *Geology* 17, 1076–1079. https://doi.org/10.1130/0091-7613(1989)017<1076:UPAOTB>2.3.CO;2

Petterson M.G. & Windley B.F. 1992: The field relationships, geochemistry and petrogenesis of the Cretaceous basalt Jutal dyke suite, Kohistan, N. Pakistan. *Journal of the Geological Society* 149, 107–114. https://doi.org/10.1144/gsjgs.149.1.0107

Plašienka D., Grecula P., Putiš M., Kováč M. & Hovorka D. 1997: Evolution and structure of the Western Carpathians: an overview. In: Grecula P., Hovorka D. & Putiš M. (Eds.): Geological Evolution of the Western Carpathians. *Mineralia Slovaca – Monograph*, Bratislava, 1–24i.

Putiš M., Nemec O., Danišík M., Jourdan F., Soták J., Tomek Č., Ružička P. & Molnárová A. 2021: Formation of a Composite Albian–Eocene Orogenic Wedge in the Inner Western Carpathians: P–T Estimates and 40Ar/39Ar Geochronology from Structural Units. *Minerals* 11, 988. https://doi.org/10.3390/min11090988

Pyle J.M., Spear F.S., Rudnick R.L. & McDonough W.F. 2001: Monazite–xenotime garnet equilibrium in metapelites and a new monazite–garnet thermometer. *Journal of Petrology* 42, 2083–2107. https://doi.org/10.1093/petrology/42.11.2083

Rapp R.P. & Watson B. 1986: Monazite solubility and dissolution kinetics: implications for the thorium and light rare earth chemistry of felsic magmas. *Contributions to Mineralogy and Petrology* 94, 304–316. https://doi.org/10.1007/BF00371439
Roberts N.M.W., Thomas R.J. & Jacobs J. 2016: Geochronological constraints on the metamorphic sole of the Semail ophiolite in the United Arab Emirates. *Geoscience Frontiers* 7, 609–619. https://doi.org/10.1016/j.gsf.2015.12.003
Rolland Y., Pêcher A. & Picard C. 2000: Middle Cretaceous back–arc formation and arc evolution along the Asian margin: the Shyok Suture Zone in northern Ladakh (NW Himalaya). *Tectonophysics* 325, 145–173. https://doi.org/10.1016/S0040-1951(00)00135-9
Rolland Y., Mahéo G., Guillot S. & Pêcher A. 2001: Tectono-metamorphic evolution of the Karakorum Metamorphic complex (Dassu-Askole area, NE Pakistan): exhumation of mid-crustal HT-MP gneisses in a convergent context. *Journal of Metamorphic Geology* 19, 717–737. https://doi.org/10.1046/j.0263-4929.2001.00342.x
Rolland Y., Pêcher A., Picard C., Lapierre H., Bosch D. & Keller F. 2002: The Ladakh Arc of NW Himalaya – slab melting and melt–mantle interaction during fast northward drift of Indian Plate. *Chemical Geology* 182, 139–178. https://doi.org/10.1016/S0009-2541(01)00286-8
Rolland Y., Carrio-Schaffhauser E., Sheppard S.M.F., Pêcher A. & Esclauze L. 2006: Metamorphic zoning and geodynamic evolution of an inverted crustal section (Karakorum margin, N Pakistan), evidence for two metamorphic events. *International Journal of Earth Sciences* 95, 288–305. https://doi.org/10.1007/s00531-005-0026-x
Rubatto D., Williams I.S. & Buick I.S. 2001: Zircon and monazite response to prograde metamorphism in the Reynolds Range, central Australia. *Contributions to Mineralogy and Petrology*, 140, 458–468. https://doi.org/10.1007/PL00007673
Santos F.H., Amaral W.S., Uchôa Filho E.C. & Martins, D.T. 2017: Detrital zircon U–Pb ages and whole–rock geochemistry of the Neoproterozoic Paulistana and Santa Filomena complexes, Borborema Province, northeastern Brazil: implications for source area composition, provenance, and tectonic setting. *International Geology Review* 59, 1861–1884. https://doi.org/10.1080/00206814.2017.1300074
Schärer U., Copeland P., Harrison T.M. & Searle M.P. 1990: Age, cooling history and origin of post–collisional leucogranites in the Karakoram batholith, a multisystem isotope study. *Journal of Geology* 98, 233–251. https://doi.org/10.1086/629395
Schmid S.M., Bernoulli D., Fügenschuh B., Matenco L., Schefer S., Schuster R., Tischler M. & Ustaszewski K. 2008: The Alpine–Carparthian–Dinaric orogenic system: Compilation and evolution of tectonic units. *Swiss Journal of Geosciences* 101, 139–183. https://doi.org/10.1007/s00015-008-1247-3
Searle M.P. 1991: Geology and tectonics of the Karakoram Mountains. *J. Wiley and Sons*, Chichester, 1–358.
Searle M.P. 2011: Geological evolution of the Karakoram Ranges. *Italian Journal of Geosciences* 130, 147–159.
Searle M.P. & Tirrul R. 1991: Structural and thermal evolution of the Karakoram crust: Geological Society of London Journal, 148, 65–82. https://doi.org/10.1144/gsjgs.148.1.0065
Searle M.P., Rex A.J., Tirrul R., Rex D.C., Barnicoat A. & Windley B.F. 1989: Metamorphic, magmatic and tectonic evolution of the central Karakoram in the Biafo–Baltoro–Hushe regions of N. Pakistan. *Geological Society of America, Special Paper* 232, 47–73. https://doi.org/10.1130/SPE232-p47
Searle M.P., Crawford M.B. & Rex A.J. 1992: Field relations, geochemistry and emplacement of the Baltoro granite, Central Karakoram. Transactions of the Royal Society, Edinburgh: *Earth Sciences* 83, 519–538. https://doi.org/10.1017/S0263593300005861
Searle M.P., Waters D.J., Dransfield M.W., Stephenson B.J., Walker C.B., Walker J.D. & Rex D.C. 1999: Thermal and mechanical models for the structural and metamorphic evolution of the Zanskar High Himalaya. In: Mac Niocaill C.& Ryan P.D. (Eds.): Continental Tectonics. *Geological Society of London, Special Publication* 164, 139–156. https://doi.org/10.1144/GSL.SP.1999.164.01.08
Searle M.P., Parrish R.R., Thow A.V., Noble S.R., Phillips R.J. & Waters D.J. 2010: Anatomy, age and evolution of a collisional mountain belt: the Baltoro granite batholith and Karakoram Metamorphic Complex, Pakistani Karakoram. *Journal of the Geological Society* 167, 183–202. https://doi.org/10.1144/0016-76492009-043
Smith H.A. 1993: Characterization and Timing of Metamor phism Within the Indo-Asian Suture Zone, Himalayas, Northern Pakistan. *PhD thesis, Dartmouth College*, Hanover, New Hampshire.
Soret M., Larson K.P., Cottle J.M., Smit M., Johnson A., Shrestha S., Ali A. & Faisal S. 2019: Mesozoic to Cenozoic tectono-metamorphic history of the South Pamir–Hindu Kush (Chitral, NW Pakistan): Insights from phase equilibria modelling, and garnet–monazite petrochronology: *Journal of Metamorphic Geology* 37, 633–666. https://doi.org/10.1111/jmg.12479
Spear F.S. & Pyle J.M. 2002: Apatite, monatite, and xenotime in metamorphic rocks. *Reviews in Mineralogy and Geochemistry* 48, 293–336. https://doi.org/10.1515/9781501509636-010
Stacey J.S. & Kramers J.D. 1975: Approximation of terrestrial lead isotope evolution by a two-stage model. *Earth and Planetary Science Letters* 26, 207–221. https://doi.org/10.1016/0012-821X(75)90088-6
Villa I.M., Lemennicier Y. & Le Fort P. 1996: Late Miocene to Early Pliocene tectonometamorphism and cooling in south central Karakorum and Indus-Tsangpo suture, Chogo Lung ma area (NE Pakistan). *Tectonophysics* 260, 201–214. https://doi.org/10.1016/0040-1951(96)00086-8
Weinberg R.F., Dunlap W.J., & Whitehouse M. 2000: New field, structural and geochronological data from the Shyok and Nubra valleys, northern Ladakh: linking Kohistan to Tibet. *Geological Society, London, Special Publications*. https://doi.org/10.1144/gsl.sp.2000.170.01.14
Wing B.A., Ferry J.M. & Harrison T.M. 2003: Prograde destruction and formation of monazite and allanite during contact and regional metamorphism of pelites: petrology and geochronology. *Contributions to Mineralogy and petrology* 145, 228–250. https://doi.org/10.1007/s00410-003-0446-1
Yang P.S. & Pattison D. 2006: Genesis of monazite and Y zoning in garnet from the Black Hills, South Dakota. *Lithos* 88, 233–253. https://doi.org/10.1016/j.lithos.2005.08.012